Vol 11 No 4, April 2002
1009-1963/2002/11(04)/0346-06

Chinese Physics

© 2002 Chin. Phys. Soc.
and IOP Publishing Ltd

Constructive interference via collision-aided radiative excitation*

Yang Xi-Hua(杨希华)†, Sun Zhen-Rong(孙真荣),
Ding Liang-En(丁良恩), and Wang Zu-Geng(王祖赓)
Key Laboratory of Optical and Magnetic Resonance Spectroscopy, and Department of Physics, East China Normal University, Shanghai 200062, *China*

(Received 20 May 2001; revised manuscript received 8 December 2001)

We have studied theoretically constructive interference via collision-aided radiative excitation in an open four-level system using a density matrix approach. The four-level system consists of a Λ-type three-level quantum-beat configuration driven by one laser field and a fourth level coupled by a vacuum mode. It is shown that through the incoherent process (collision), coherence between widely-separated doublets and subsequent constructive interference can be realized. We analyse the effects of the collision-induced coherent and incoherent decay rates, laser intensity, and energy separation of the doublets on the interference. Meanwhile, the constructive interference between the two transition pathways $3P_{1/2}$–4D and $3P_{3/2}$–4D via equal-frequency hybrid excitation and collision-aided radiative excitation in an Na_2-Na system is experimentally observed. A good agreement between the theoretical and experimental results is obtained.

Keywords: constructive interference, collision-aided radiative excitation, hybrid excitation
PACC: 4250, 3280, 3400, 4225H

1. Introduction

Quantum coherence and interference phenomena have attracted considerable interest in recent years, since these give rise to many novel effects, such as spontaneous emission cancellation,[1–3] electromagnetically induced transparency,[4] coherent population trapping,[5,6] laser without inversion,[7,8] and strong narrowing of spectral line.[9–11] The nature of the quantum interference (constructive or destructive) depends not only on atomic structures and parameters, but also on experimental conditions, such as the dephasing collision. Destructive interference has been extensively studied,[1–8] whereas only a few studies have been carried out for constructive interference.[12,13] In addition, most of the previous theoretical studies have focused on a closed system. In fact, the atomic or molecular system (especially the excited one) is an open system, but there have only been a few studies on this.[14]

In the V-type or Λ-type quantum-beat configurations, quantum interference relies on the establishment of coherent superposition between doublets. The coherence between very narrow-spaced doublets can be realized easily through various coherent methods.[15] It seems difficult to create coherence between a doublet with a large energy separation. Nevertheless, an incoherent process (collision) can create coherence between the widely-separated doublets, which has been theoretically studied in pressure-induced extra resonances in nonlinear spectroscopy.[16] Similar coherent effects induced by collisional relaxation have been observed in pressure-induced extra resonances in four-wave mixing.[17]

In this paper, we study theoretically the collision-induced coherence and constructive interference in an open four-level system based on our experimental observation of the constructive interference between two transition pathways $3P_{1/2}$–4D and $3P_{3/2}$–4D via equal-frequency hybrid excitation (EFHE)[18] and collision-aided radiative excitation (CARE)[19,20] in an Na_2–Na system. By using the density matrix approach, the effects of the collision-induced coherent and incoherent decay rates, laser intensity, and energy separation of the doublets on the interference are analysed.

2. Equation of motion

Figure 1 shows the open four-level model. The

*Project supported by the National Natural Science Foundation of China (Grant Nos 19734003 and 10074015).
†+021-62232453(O), 021-62232453(FAX), email:yangxih@yahoo.com.cn

common upper level 1 is driven by a laser field to the lower widely-separated doublets 2 and 3, and coupled to a fourth level 4 by a vacuum mode. We consider that levels 1, 2, 3 and 4 correspond to the sodium atom levels 4D, $3P_{3/2}$, $3P_{1/2}$ and 4P, respectively, and we study the interference between two transition pathways 2–1 and 3–1 via CARE. Since the intensity of 1–4 emission is proportional to the population of level 1, we can measure the excitation spectrum for generating 1–4 emission to test the two transitions 2–1 and 3–1 via CARE and the interference. The laser field with an amplitude E couples level 1 and levels 3 and 2 with Rabi frequencies $\Omega_1 = \mu_1 \cdot E/\hbar$ and $\Omega_2 = \mu_2 \cdot E/\hbar$, where μ_1 and μ_2 are the dipole moments for transitions 3–1 and 2–1, respectively. The detunings of the laser from atomic resonant transitions 3–1 and 2–1 are given by $\Delta_1 = \omega_L - \omega_{13}$ and $\Delta_2 = \omega_L - \omega_{12}$, respectively, where $\omega_{ij} (i \neq j)$ is the atomic resonant frequency between levels i and j, and ω_L is the laser frequency. We denote $\Delta = \omega_L - \omega_{13} + \omega_{23}/2$ as the detuning of the laser from the middle position of the two atomic resonant transition frequencies ω_{12} and ω_{13}. $2\gamma_1$, $2\gamma_2$ and $2\gamma_3$ are the population decay rates from level 1 to levels 3, 2 and 4, respectively; $2\gamma_a$, $2\gamma_b$, and $2\gamma_c$ are the population decay rates from levels 4, 3 and 2 to other lower levels, respectively, which may exist in the real open atomic system. The relaxation rates of the atomic level population and coherence are denoted by γ_{ii} and γ_{ij} $(i \neq j)$, respectively. Apart from the radiative relaxation, the atom also undergoes collision due to the addition of a buffer gas. The collision-induced coherence decay rate between levels i and j is denoted by γ_{ijp} $(i \neq j)$, and the collision-induced population transfer rate between the doublets 2 and 3 is denoted by $2\gamma_0$. γ_τ is the escape rate of the atomic system; R_b and R_c are the atomic injection rates to populate levels 3 and 2 through some incoherent pumping process, such as the Na_2^*–Na collision-induced energy-transfer in our experiment. By applying the slowly-varying amplitude and rotating-wave approximation, equations for the density matrix elements can be written as

$$\dot{\rho}_{11} = -\gamma_{11}\rho_{11} + i\Omega_1(\rho_{31} - \rho_{13}) + i\Omega_2(\rho_{21} - \rho_{12}), \tag{1}$$

$$\dot{\rho}_{22} = 2\gamma_2\rho_{11} + 2\gamma_0\rho_{33} - \gamma_{22}\rho_{22} + i\Omega_2(\rho_{12} - \rho_{21}) + R_c, \tag{2}$$

$$\dot{\rho}_{33} = 2\gamma_1\rho_{11} + 2\gamma_0\rho_{22} - \gamma_{33}\rho_{33} + i\Omega_1(\rho_{13} - \rho_{31}) + R_b, \tag{3}$$

$$\dot{\rho}_{44} = 2\gamma_3\rho_{11} - 2\gamma_a\rho_{44}, \tag{4}$$

$$\dot{\rho}_{12} = -\left(\gamma_{12} - i\left(\Delta + \frac{\omega_{23}}{2}\right)\right)\rho_{12} + i\Omega_1\rho_{32} + i\Omega_2(\rho_{22} - \rho_{11}), \tag{5}$$

$$\dot{\rho}_{13} = -\left(\gamma_{13} - i\left(\Delta + \frac{\omega_{23}}{2}\right)\right)\rho_{13} + i\Omega_2\rho_{23} + i\Omega_1(\rho_{33} - \rho_{11}), \tag{6}$$

$$\dot{\rho}_{14} = -\gamma_{14}\rho_{14} + i\Omega_2\rho_{24} + i\Omega_1\rho_{34}, \tag{7}$$

$$\dot{\rho}_{23} = -(\gamma_{23} + i\omega_{23})\rho_{23} - i\Omega_1\rho_{21} + i\Omega_2\rho_{13}, \tag{8}$$

$$\dot{\rho}_{24} = -\left(\gamma_{24} + i\left(\Delta + \frac{\omega_{23}}{2}\right)\right)\rho_{24} + i\Omega_2\rho_{14}, \tag{9}$$

$$\dot{\rho}_{34} = -\left(\gamma_{24} + i\left(\Delta - \frac{\omega_{23}}{2}\right)\right)\rho_{34} + i\Omega_1\rho_{14}, \tag{10}$$

where

$$\gamma_{11} = 2\gamma_1 + 2\gamma_2 + 2\gamma_3 + \gamma_\tau,$$

$$\gamma_{22} = 2\gamma_c + 2\gamma_0 + \gamma_\tau,$$

$$\gamma_{33} = 2\gamma_b + 2\gamma_0 + \gamma_\tau,$$

$$\gamma_{44} = 2\gamma_a + \gamma_\tau,$$

$$\gamma_{12} = \gamma_1 + \gamma_2 + \gamma_3 + \gamma_c + \gamma_0 + \gamma_{12p},$$

$$\gamma_{13} = \gamma_1 + \gamma_2 + \gamma_3 + \gamma_b + \gamma_0 + \gamma_{13p},$$

$$\gamma_{14} = \gamma_1 + \gamma_2 + \gamma_3 + \gamma_a,$$

$$\gamma_{23} = \gamma_b + \gamma_c + 2\gamma_0 + \gamma_{23p},$$

$$\gamma_{24} = \gamma_c + \gamma_a + \gamma_0,$$

$$\gamma_{34} = \gamma_b + \gamma_a + \gamma_0.$$

The above density-matrix equations can be written in a compact form

$$\frac{\mathrm{d}}{\mathrm{d}t}\varphi(t) = L\varphi(t) + I, \tag{11}$$

where φ is a column vector, whose elements are defined by $\varphi_1 = \rho_{11}$, $\varphi_2 = \rho_{12}$, $\varphi_3 = \rho_{13}$, $\varphi_4 = \rho_{14}$, $\varphi_5 = \rho_{21}$, $\varphi_6 = \rho_{22}$, $\varphi_7 = \rho_{23}$, $\varphi_8 = \rho_{24}$, $\varphi_9 = \rho_{31}$, $\varphi_{10} = \rho_{32}$, $\varphi_{11} = \rho_{33}$, $\varphi_{12} = \rho_{34}$, $\varphi_{13} = \rho_{41}$, $\varphi_{14} = \rho_{42}$, $\varphi_{15} = \rho_{43}$, $\varphi_{16} = \rho_{44}$, and the vector I is an inhomogeneous term with $I_6 = R_b$, $I_{11} = R_c$. L is a 16×16 matrix containing the coefficients of the matrix equations, which is too bulky to be presented here, but it can be easily derived from the matrix equations. The intensity of the emission spectrum for 1–4 transition is proportional to the Fourier transform of the two-time correlation function

$$\Gamma(t,\tau) = \langle P^{(-)}(t+\tau)\cdot P^{(+)}(\tau)\rangle, \qquad (12)$$

where $\boldsymbol{P}^{(-)} = \mu_{14}|1\rangle\langle 4|$ and $\boldsymbol{P}^{(+)}=[\boldsymbol{P}^{(-)}]^{+}$ are the negative and positive frequency parts of the polarization operator for 1–4 transition, respectively. As performed in Ref.[9], with the help of the quantum regression theorem, the emission spectrum for 1–4 transition in a steady state is given by

$$S(\omega) = \mathrm{Re}\Gamma(z)|_{z=i\omega}, \qquad (13)$$

where

$$\begin{aligned}\Gamma(z) =&\mu_{14}^2[M_{13,13}(z_1)\varphi_1(\infty) + M_{13,14}(z_1)\varphi_2(\infty)\\ &+ M_{13,15}(z_1)\varphi_3(\infty) + M_{13,16}(z_1)\varphi_4(\infty)\\ &+ \sum_{j=1}^{16} N_{13,j}(z_1)\cdot I_j\varphi_4(\infty), \end{aligned}\qquad (14)$$

with $z_1 = z - i\omega_{14}$ and $\varphi(\infty) = -L^{-1}I$. The matrices M and N are defined as $M(z) = (z-L)^{-1}$ and $N(z) = L^{-1}(z-L)^{-1}$, respectively. The excitation spectrum for generating 1–4 emission can be obtained by fixing the emission frequency $\omega = \omega_{14}$ and tuning the laser frequency, which is denoted by $S(\Delta)$=Re$\Gamma(z,\Delta)|z = i\omega_{14}$.

3. Results and discussion

The above simple theory can be readily applied to the prediction of the position and shape of the interference signal. It is well known that the quantum interference in a Λ-type three-level quantum-beat configuration relies on the establishment of the coherent superposition between the two doublets 2 and 3. As is seen clearly from Eqs.(5) and (6), the coherence should result from the nonzero coherent terms ρ_{23} and ρ_{32}. Without the coherence, the excitation spectrum would only consist of two peaks corresponding to the two independent absorption 2–1 and 3–1. In the following calculations, the relative parameters are scaled with cm^{-1} and set according to the levels of sodium atom in the inset in Fig.1. The population decay rates are taken from Refs.[21] and [22]. For simplicity, we assume that the dipole moments of the two transitions 2–1 and 3–1 are equal.

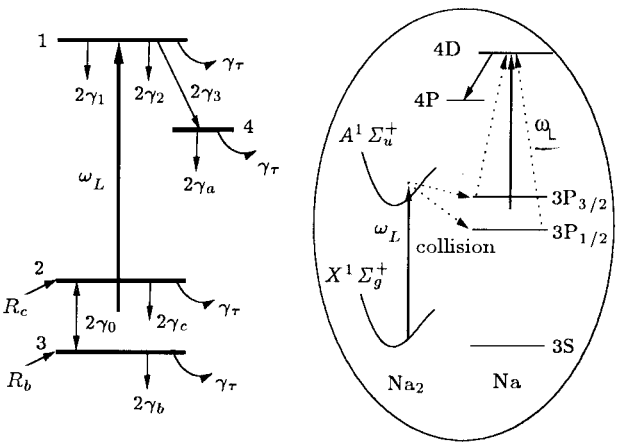


Fig.1. The open four-level model, where levels 1, 2, 3 and 4 correspond to sodium atom levels 4D, $3P_{3/2}$, $3P_{1/2}$, and 4P, respectively. The inset shows the relevant energy levels of Na_2–Na and the equal-frequency hybrid excitation process. The two dashed lines indicate two transitions $3P_{1/2}$–4D and $3P_{3/2}$–4D through CARE.

The excitation spectra $S(\Delta)$ in Fig.2 display the dependence of the interference on the collision-induced coherent decay rate γ_{ijp} and incoherent escape rate γ_τ. It can be seen that, when the decay rate γ_{ijp} is relatively small and the escape rate γ_τ is relatively large, there are only two side peaks corresponding to the resonant absorptions 2–1 and 3–1, respectively. With the increase of the decay rate γ_{ijp}, the interference peak grows stronger and stronger, and would be much stronger than the two side peaks. Meanwhile, the width of the interference peak is far narrower than those of the two side peaks. However, if the incoherent escape rate γ_τ increases, the interference peak would decrease and disappear eventually. In a moderate range of the decay rates γ_{ijp} and γ_τ, the larger the collision-induced coherent decay rate γ_{ijp} and the smaller the escape rate γ_τ, the stronger the interference signal. It is shown that the collision-induced decay rate γ_{ijp} plays an important role in the coherence and interference. In the case of the widely-separated doublets 2 and 3, as analysed by Grynberg and Berman[16] the coherence between the doublets comes from the collision-induced nonzero coherent terms ρ_{23} and ρ_{32}, which critically depends on the collision-induced coherent decay rate γ_{ijp}. The larger

the decay rate γ_{ijp}, the stronger the coherence between the doublets. Therefore, the interference peak would grow stronger with increasing decay rate γ_{ijp}. On the other hand, the increase of the dephasing escape rate γ_τ would destroy the coherence and eventually results in the disappearance of the interference.

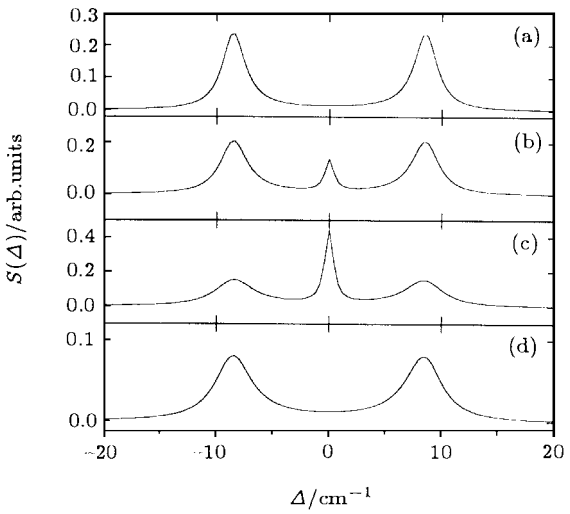


Fig.2. The excitation spectra $S(\Delta)$ for different collision-induced coherent decay rates γ_{ijp} and escape rates γ_τ: ω_{23}=17.2, $\gamma_2 = \gamma_1$=0.00011, γ_3=0.00012, γ_a=0.00015, $\gamma_b = \gamma_c$=0.001, $\Omega_1 = \Omega_2$=0.5, $R_b = R_c$=0.5, γ_o=0.4, $\gamma_{12p} = \gamma_{13p}$=1.2$p$, γ_{23p}= 3.2p (p represents the relative buffer gas pressure). (a) p=0.51, γ_τ=2, (b) p=0.7, γ_τ=2, (c) p=1.2, γ_τ=2, (d) p=1.2, γ_τ=3.6.

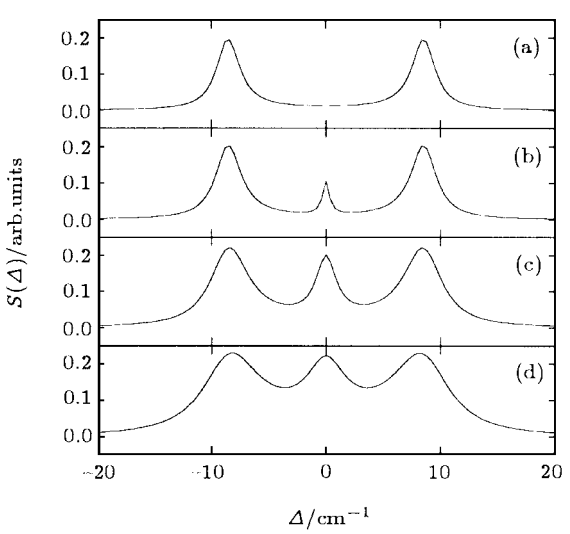


Fig.3. The excitation spectra $S(\Delta)$ for different collision-induced population transfer rate γ_0: (a) γ_0=0.16, (b) γ_0=0.3, (c) γ_0=1, (d) γ_0=2. p=0.7, γ_τ=2, and the other parameters are the same as those in Fig.2.

The excitation spectra $S(\Delta)$ in Fig.3 show the dependence of the interference on the collision-induced population transfer rate γ_0. It can be seen that, when the population transfer rate γ_0 is relatively small, there are only two side peaks. With the increase of γ_0, the interference peak grows stronger and becomes wider. When the population transfer rate γ_0 is relatively large, the interference peak almost has the same strength and width as the two side peaks, and the background becomes very wide and strong. This indicates that the coherence and interference effect depends on the collision-induced population transfer rate γ_0, as well as the collision-induced coherent decay rate γ_{ijp}. The increase of the population transfer rate γ_0 would not only enhance the coherence and interference effect, but also broaden the interference peak and background.

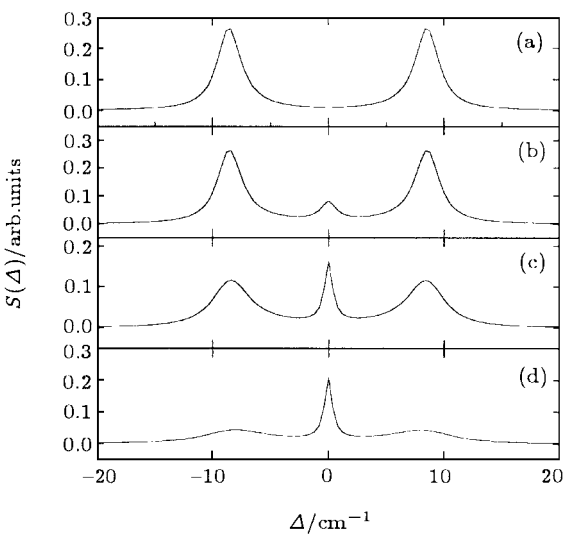


Fig.4. The excitation spectra $S(\Delta)$ for different Rabi frequencies of the laser field: (a) $\Omega_1 = \Omega_2$=0.05, (b) $\Omega_1 = \Omega_2$=0.2, (c) $\Omega_1 = \Omega_2$=1, (d) $\Omega_1 = \Omega_2$=2. p=0.7, γ_τ=2, and the other parameters are the same as those in Fig.2.

Figure 4 shows the excitation spectra $S(\Delta)$ for different Rabi frequencies of the laser field. It can be seen that, when the laser Rabi frequency is very small, only two side peaks can exist. With the increase of the laser Rabi frequency, the interference signal becomes stronger and its width becomes narrower. When the laser Rabi frequency is relatively large, but still much smaller than the energy separation of the doublets, the interference peak becomes far stronger than the two side peaks. In the perturbation limit, the collision-induced coherence appears in the second-order density matrix elements $\rho_{23}^{(2)}$ and $\rho_{32}^{(2)}$, and the coherence-induced contribution to level 1 population appears in the fourth order. Therefore, the interference is very sensitive to the laser Rabi frequency. When the laser

intensity is very low, the coherence is very weak and only two side peaks exist. With the increase of the laser intensity, the coherence between the doublets becomes strong, and the subsequent constructive interference results in the enhancement of absorption. When the laser intensity is relatively large, the coherence is so strong that the contribution of coherence to level 1 population would be much larger than that resulting from the two resonant absorptions.

The dependence of the interference on the energy separation of the doublets 2 and 3 is shown in Fig.5. It can be seen that when the energy separation of the doublets is too small, the two side peaks turn into one broad emission peak due to the collision broadening. With the increase of the energy separation, the interference peak and the two side peaks become separated. When the energy separation is relatively large, e.g. ω_{23}=70cm^{-1}, the interference peak becomes very weak and its width becomes broad. However, if the collision-induced coherent decay rate γ_{ijp} or the population transfer rate γ_0 increases, the interference peak would grow strong again. This clearly indicates that, through the incoherent process (collision), the coherent superposition between the widely-separated doublets can be established. Note that when the energy separation of the doublets is so wide that the collision could not enable both transitions 2–1 and 3–1 to take place simultaneously, the interference would disappear.

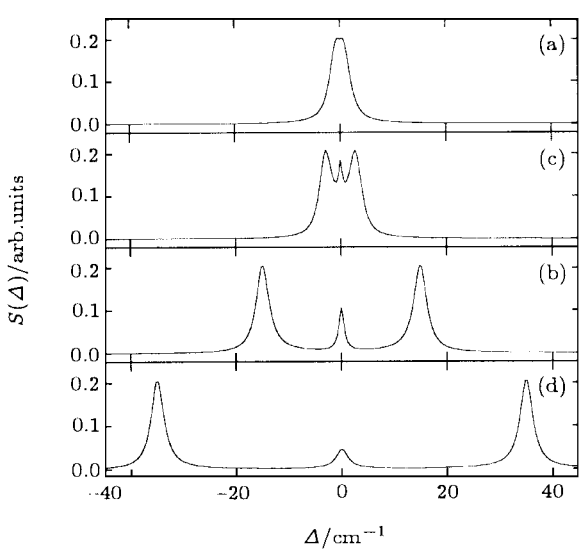


Fig.5. The excitation spectra $S(\Delta)$ for different energy separations of the doublets: (a) ω_{23}=2, (b) ω_{23}=6, (c) ω_{23}=30, (d) ω_{23}=70. p=0.7, γ_τ=2, and the other parameters are the same as those in Fig.2.

The inset in Fig.1 schematically shows the experimental relevant energy levels in the Na_2–Na system together with the equal-frequency hybrid excitation and stimulated emission 4D–4P. The hybrid excitation includes two processes.[18] The first process is the excitation of Na_2 from $X^1\sum_g^+$ to $A^1\sum_u^+$ state, and the subsequent Na_2^*–Na collision-induced energy-transfer to populate $3P_{1/2}$ and $3P_{3/2}$ levels. The second process is the resonant excitation or the CARE of a sodium atom from $3P_{1/2,3/2}$ levels to the 4D level. Both processes are driven by the same laser. In the second excitation process, the doublets $3P_{1/2,3/2}$ and level 4D form a Λ-type quantum-beat configuration. Under certain conditions, both transitions $3P_{1/2}$–4D and $3P_{3/2}$–4D can take place simultaneously through the CARE and will interfere with each other. The experimental set-up is about the same as that in a previous experiment.[23] The dye laser pumped by a Q-switched Nd:YAG laser with a pulse duration of about 12 ns and a linewidth 0.1cm^{-1} is tuned in the measuring range of 567.8~570.0nm. The forward infrared stimulated emission 4D–4P at 2.34μm is detected to test the $3P_{1/2,3/2}$–4D transitions and the interference.

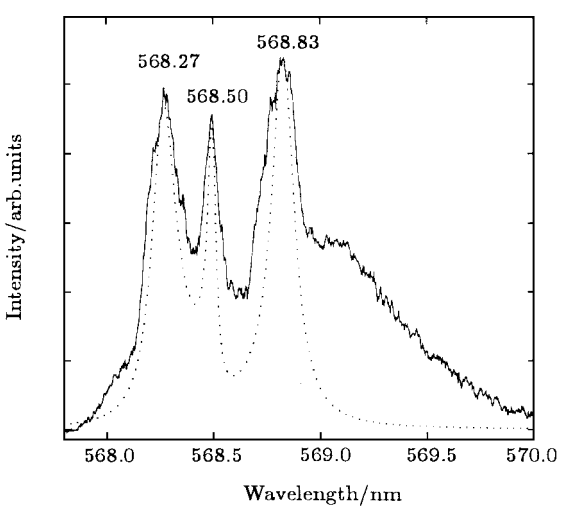


Fig.6. Calculated (dotted line) and experimental (solid line) excitation spectra for generating the stimulated emission 4D–4P at 2.34μm with the buffer gas 0.2 bar, sample temperature 700K, and pulse energy 2.0mJ.

The solid line in Fig.6 shows the excitation spectrum for generating the infrared stimulated emission 4D–4P. It can be seen that there are three sharp peaks on the broad background (between 568.0nm and 569.8nm). The two side peaks result from the two atomic resonant absorptions $3P_{1/2}$–4D and $3P_{3/2}$–4D with excitation wavelengths 568.27nm and 568.83nm, respectively. The excitation wavelength at 568.50nm

for the middle narrow peak does not coincide with any resonant transition wavelengths of sodium atom. The most distinct feature of the quantum interference signal is that its position is determined by the ratio of the dipole moments of the two corresponding transitions, i.e. $\mu_1^2\Delta_2 + \mu_2^2\Delta_1 = 0$.[1−3] Another feature is its narrow width, indicating the slow decay rate of the atomic coherent state. As is shown in Fig.6, the ratio of the detunings of the middle narrow peak from the right and left peaks is about 1.4, which is equal to the reverse ratio of the two transition probabilities (the transition probabilities taken from Ref.[24]). That is, the ratio is proportional to the square of the reverse ratio of the two transition dipole moments. This indicates that the middle narrow peak results from the constructive interference between the two transition pathways $3P_{1/2}$–4D and $3P_{3/2}$–4D. The dotted line in Fig.6 is the calculated curve for $S(\Delta)$. The parameters are set according to the experimental conditions as follows: $\Omega_2 = \sqrt{1.4}\Omega_1 = 0.5$, $\gamma_0 = 0.4$, $\gamma_{12p} = 1.4$, $\gamma_{13p} = 1.2$, $\gamma_{23p} = 3.8$, $\gamma_\tau = 2.7$. Note that the ratio of the Rabi frequencies Ω_2 and Ω_1 equals the ratio of the two transition dipole moments μ_2 and μ_1. Both the calculated and experimental results show a narrow peak standing at the place where the condition for quantum interference is satisfied. A good agreement between theory and experiment is obtained.

In the above theoretical calculation, we set γ_0 to be about twice as large and γ_{ijp} to be about one and a half times as large as those calculated with the parameters in Refs.[25] and [26], respectively. The escape rate γ_τ is a fitting parameter, in which we take into account the sources for depopulating the atomic system, such as collision-quenching, collision-pooling, as well as the escape of the atom out of the laser beam. The above calculations also include the laser linewidth, which can be phenomenologically added to the decay rates of the off-diagonal density matrix elements if the laser line shape is regarded as Lorentzian.[27]

4. Conclusions

We have studied theoretically the collision-induced coherence and constructive quantum interference in an open four-level system. An agreement between the theoretical and experimental results is obtained. It is shown that, through the incoherent process (collision), the coherence between the widely-separated doublets and subsequent constructive interference can be realized. Our results could pave the way for further studies of the interference through incoherent excitation processes.

References

[1] Cardimona D A, Raymer M G and Stroud Jr C R 1982 *J. Phys. B: At. Mol. Phys.* **15** 55

[2] Xia H R, Ye C R and Zhu S Y 1996 *Phys. Rev. Lett.* **77** 1032

[3] Zhu S Y and Scully M O 1996 *Phys. Rev. Lett.* **76** 388

[4] Harris S E 1997 *Phys. Today* **50** 36

[5] Arimondo E 1996 *Prog. Opt.* 35 257

[6] Li G X, Huang G M and Peng J S 1998 *Chin. Phys.* **7** 662

[7] Kocharovskaya O A 1992 *Phys. Rep.* **219** 175

[8] Luo Z F and Xu Z Z 1992 *Phys. Rev.* A **45** 8292

[9] Narducci L M, Scully M O, Oppo G L, Ru P and Tredicce J R 1990 *Phys. Rev.* A **42** 1630

[10] Gauthier D J, Zhu Y F and Mossberg T W 1991 *Phys. Rev. Lett.* **66** 2460

[11] Zhou P and Swain S 1997 *Phys. Rev.* A **56** 3011

[12] Agarwal G S 1997 *Phys. Rev.* A **55** 2467

[13] Akulshin A M, Barreiro S and Lezama A 1998 *Phys. Rev.* A **57** 2996

[14] Zhu S Y, Wang D Z and Gao J Y 1997 *Phys. Rev.* A **55** 1339

[15] Fleischhauer M, Keitel C H, Scully M O, Su C, Ulrich B T and Zhu S Y 1992 *Phys. Rev.* A **46** 1468

[16] Grynberg G and Berman P R 1990 *Phys. Rev.* A **41** 2677

[17] Prior Y, Bogdan A R, Dagenais M and Bloembergen N 1981 *Phys. Rev. Lett.* **46** 111

[18] Wang Z G and Xia H R 1991 *Molecular and Laser Spectroscopy* (Berlin: Springer) p 174

[19] Carlsten J L, Szoke A and Raymer M G 1977 *Phys. Rev.* A **15** 1029

[20] Yeh S and Berman P R 1979 *Phys. Rev.* A **19** 1106

[21] Lindgard A and Nielsen S E 1977 *At. Data Nucl. Data Tables* **19** 533

[22] Radzig A A and Smirnov B M 1985 *Reference Data on Atoms, Molecules and Ions* (Berlin: Springer)

[23] Tang X L, Wang Z G, Zhang K C, Qin L J and Cheng I S 1988 *Acta Phys. Sin.* **37** 1227 (in Chinese)

[24] Sobelman I I 1978 *Atomic Spectra and Radiative Transitions* (Berlin: Springer) p 299

[25] Lewis E L 1980 *Phys. Rev.* **58** 47

[26] Allard N and Kielkopf J 1982 *Rev. Mod. Phys.* **54** 1103

[27] Gea-Banacloche J, Li Y Q, Jin S Z and Xiao M 1995 *Phys. Rev.* A **95** 576